Polarization in the Elastic Scattering of Deuterons from Complex Nuclei in the Energy Region 94 to 157 Mev*

JOHN BALDWIN, OWEN CHAMBERLAIN, EMILIO SEGRÈ, ROBERT TRIPP, CLYDE WIEGAND, AND THOMAS YPSILANTIS
Radiation Laboratory and Department of Physics, University of California, Berkeley, California
(Received May 31, 1956)

The elastic double scattering of deuterons by complex nuclei has been investigated experimentally. Measurements were made on carbon, aluminum, and copper near 157 Mev, on lithium, beryllium, and carbon near 125 Mev, and on carbon and aluminum at 94 Mev. The expected tensor components of the deuteron polarization have not been found. Measurements have been made of the differential cross section and vector-type polarization as a function of angle. The observed polarizations were found to be larger than would be expected on the basis of the individual nucleon-nucleus interactions.

1. INTRODUCTION

BOTH in its experimental and theoretical features, the double scattering of deuterons is more complicated than nucleon-nucleus double scattering. The second-scattered intensity of nucleons may be described by but one parameter in addition to the unpolarized cross section—namely, the polarization. For deuterons, however, because they have spin 1, four additional parameters may in principle be measured. The theoretical treatment of deuteron scattering must of necessity entail more approximations than that for protons because the deuteron is not an "elementary" particle. The problem is further complicated by the existence of both S and D states in the deuteron wave function.

In spite of the theoretical difficulties, the results of the experiments should lead to a better understanding of the nature of the spin-orbit interaction[1] which is assumed to give rise to polarization phenomena, and of the energy dependence of the nucleon-nucleus interaction.[2]

The results of some earlier deuteron experiments at this laboratory have been reported in *The Physical Review*.[3] Lakin[4] has given a theoretical discussion of deuteron double scattering. Stapp,[5] using a formalism different from that of Lakin, has made an attempt to fit some of the present data. He has considered first and second Born approximations as well as contributions due to the presence of D state in the deuteron wave function.

Throughout this paper the symbol Θ is used to denote the (polar) scattering angle as measured in the laboratory system, and θ for that measured in the center-of-mass system.

2. THEORETICAL

In this section we recapitulate the theory of the spin polarization of the deuteron given by Lakin.[4]

* This work was done under the auspices of the U. S. Atomic Energy Commission.
[1] E. Fermi, Nuovo cimento 11, 407 (1954).
[2] R. M. Sternheimer, Phys. Rev. 100, 886 (1955).
[3] Chamberlain, Segrè, Tripp, Wiegand, and Ypsilantis, Phys. Rev. 95, 1104 (1954).
[4] W. Lakin, Phys. Rev. 98, 139 (1955).
[5] H. P. Stapp, University of California Radiation Laboratory Report, UCRL-3098, August, 1955 (unpublished).

The polarization state of a beam of nucleons can be completely specified by the statistical expectation values of four linearly independent matrices in the two-dimensional spin-space of the nucleon. These matrices are usually chosen to be the unit matrix, 1, and the Pauli spin matrices, σ_x, σ_y, and σ_z. By a proper choice of coordinates, the polarization state of the beam may be described by the expectation values of only two of the four matrices, namely, 1 and σ_z. In the spin-space of the deuteron there are nine linearly independent matrices. Again, the proper choice of coordinate axes allows us to specify the polarization state of a beam of deuterons by the expectation values of five of these nine. Lakin constructs a convenient complete set of nine 3×3 matrices from the unit matrix, 1, and the Cartesian components of the unit-angular-momentum operator in matrix representation, S_x, S_y, and S_z, in a manner similar to the formation of the spherical harmonics from 1, x, y, and z. These operators are denoted by T_{JM} and are defined as

$$
\begin{aligned}
T_{00} &= 1, \\
T_{11} &= -\tfrac{1}{2}\sqrt{3}(S_x + iS_y), \\
T_{10} &= (\tfrac{3}{2})^{\frac{1}{2}}S_z, \\
T_{22} &= \tfrac{1}{2}\sqrt{3}(S_x + iS_y)^2, \\
T_{21} &= -\tfrac{1}{2}\sqrt{3}[(S_x + iS_y)S_z + S_z(S_x + iS_y)], \\
T_{20} &= (\tfrac{1}{2})^{\frac{1}{2}}(3S_z^2 - 2), \\
T_{J-M} &= (-1)^M T_{JM}^{\dagger}.
\end{aligned}
\tag{2.1}
$$

J and M are simply parameters that number the matrices and have nothing to do with the angular momentum of the system.

Let us denote by $\langle T_{JM} \rangle$ the quantum-mechanical expectation value of T_{JM} averaged over the particles of a beam. For a beam of unpolarized deuterons, all the $\langle T_{JM} \rangle$ are zero except $\langle T_{00} \rangle$, the normalization. If we scatter a beam of unpolarized deuterons and examine the portion of the scattered flux in the neighborhood of some mean scattering angle, we should expect this "beam" to be characterised by some nonzero $\langle T_{JM} \rangle$, which would, of course, be functions of the scattering angle.

Consider the following double-scattering experiment. A beam of unpolarized deuterons is incident upon target No. 1, with an initial propagation vector $\mathbf{k}_{1i}$ (where the momentum of a particle is $\mathbf{p}=\hbar\mathbf{k}$). Let that portion of the scattered flux near some final propagation vector $\mathbf{k}_{1f}$ be incident upon a target No. 2. Let us measure the second scattered flux near some final propagation vector, $\mathbf{k}_{2f}$ (the initial second-scattering propagation vector, $\mathbf{k}_{2i}=\mathbf{k}_{1f}$, neglecting energy loss in the targets). If one sets up, for the second scattering, a right-handed coordinate system whose z axis is along $\mathbf{k}_{1f}$ and whose y axis is along the normal, $\mathbf{n}_1$, to the first scattering plane ($\mathbf{n}_1=\mathbf{k}_{1i}\times\mathbf{k}_{1f}$), then, as Lakin shows, the second-scattered intensity is given by[6]

$$I=I_0[1+\langle T_{20}\rangle_1\langle T_{20}\rangle_2+2(-\langle T_{21}\rangle_1\langle T_{21}\rangle_2$$
$$+i\langle T_{11}\rangle_1 i\langle T_{11}\rangle_2)\cos\phi$$
$$+2\langle T_{22}\rangle_1\langle T_{22}\rangle_2\cos2\phi]. \quad (2.2)$$

The index on T_{JM} indicates that the parameter is characteristic of either the first or second scattering. The angle ϕ between the normals to the two scattering planes is given by $\mathbf{n}_1\cdot\mathbf{n}_2=n_1n_2\cos\phi$. I_0 is the unpolarized differential-scattering cross section for the second scattering.

It is shown that if the first scattering does produce any nonzero $\langle S\rangle$, it is directed along the y axis. From Eq. (2.1) we note that $\langle T_{11}\rangle$ is pure imaginary [that is, $\langle T_{11}\rangle=-(i/2)\sqrt{3}\langle S_y\rangle$], and the $\langle T_{2M}\rangle$ are all real.

We shall refer to $i\langle T_{11}\rangle$ as the vector polarization since it is the expectation value of the y component of the vector $\mathbf{S}$. The $\langle T_{2M}\rangle$ are referred to as components of the tensor polarization, since the T_{2M} are compounded from the elements of the second-rank tensor S_iS_j.

Let us attempt to apply the impulse approximation[7-9] to a model similar to that used by Fermi[1] in connection with scattering of nucleons. If we assume charge independence, the interaction of a proton with a nucleus is identical to that of a neutron. We also assume that the Hamiltonian may be written

$$H=T_1+T_2+U_d(r_{12})+V(\mathbf{r}_1,\mathbf{p}_1,\sigma_1)+V(\mathbf{r}_2,\mathbf{p}_2,\sigma_2), \quad (2.3)$$

where 1 and 2 label the neutron and proton of the deuteron, T is the kinetic energy operator, $r_{12}=|\mathbf{r}_1-\mathbf{r}_2|$ is the separation of the nucleons of the deuteron, $U_d(r_{12})$ is the interaction between the nucleons of the deuteron, and V is the interaction of a nucleon with the target nucleus. We then write $H=H_0+H_1$, where

$$H_0=T_1+T_2+U_d(r_{12}),$$
$$H_1=V(1)+V(2). \quad (2.4)$$

The initial and final wave functions may be written

$$\psi_i=\exp[i\mathbf{k}_i\cdot\tfrac{1}{2}(\mathbf{r}_1+\mathbf{r}_2)]F(r_{12})\chi_1{}^{mi},$$
$$\psi_f=\exp[i\mathbf{k}_f\cdot\tfrac{1}{2}(\mathbf{r}_1+\mathbf{r}_2)]F(r_{12})\chi_1{}^{mf}, \quad (2.5)$$

$F(r_{12})$ is the deuteron wave function (assumed to be pure S state) and $\chi_1{}^m$ is the 3-component spinor of unit angular momentum with magnetic quantum number m. In the Born approximation, the scattering matrix M_d is given as the matrix element of H_1 connecting the initial and final eigenstates of H_0.

$$M_d=-\frac{2\mu_d}{4\pi\hbar^2}\int d\mathbf{r}_1 d\mathbf{r}_2 F^*\exp[-i\mathbf{k}_f\cdot\tfrac{1}{2}(\mathbf{r}_1+\mathbf{r}_2)]$$
$$\times[V(1)+V(2)]\cdot\exp[i\mathbf{k}_i\cdot\tfrac{1}{2}(\mathbf{r}_1+\mathbf{r}_2)]F, \quad (2.6)$$

where μ_d is the deuteron reduced mass. Let us write V as a central potential plus a spin-orbit term

$$V=U(r)+\sigma\cdot[-\nabla Y(r)]\times\mathbf{p}\lambda_c^2/\hbar, \quad (2.7)$$

where λ_c is $1/2\pi$ times the nucleon Compton wavelength, and is introduced so that Y has dimensions of energy. We then obtain for the scattering matrix the expression

$$M_d=f^{\frac{1}{2}}(K)[2g_d(K)+h_d(K,k)\mathbf{S}\cdot\mathbf{n}], \quad (2.8)$$

where $\hbar K$ is the momentum transfer of the whole deuteron in the c.m. system, $K=|\mathbf{k}_f-\mathbf{k}_i|=2k\sin(\theta/2)$, and $f(K)$ is the sticking factor.[8] In the Born approximation, g_d and h_d are given by

$$g_d(K)=-\frac{2\mu_d}{4\pi\hbar^2}\int d\mathbf{r}\,e^{-i\mathbf{K}\cdot\mathbf{r}}U(r),$$
$$h_d(K,k)=i\lambda_c^2k^2\sin\theta\left(-\frac{2\mu_d}{4\pi\hbar^2}\right)\int d\mathbf{r}\,e^{-i\mathbf{K}\cdot\mathbf{r}}Y(r). \quad (2.9)$$

The scattering matrix describing the scattering of free nucleons by the potential V of Eq. (2.7) is

$$M_n=g_n(K)+h_n(K,k)\sigma\cdot\mathbf{n}. \quad (2.10)$$

In the Born approximation, g_n and h_n are given by

$$g_n(K)=-\frac{2\mu_n}{4\pi\hbar^2}\int d\mathbf{r}\,e^{-i\mathbf{K}\cdot\mathbf{r}}U(r),$$
$$h_n(K,k)=i\lambda_c^2k^2\sin\theta\left(-\frac{2\mu_n}{4\pi\hbar^2}\right)\int d\mathbf{r}\,e^{-i\mathbf{K}\cdot\mathbf{r}}Y(r). \quad (2.11)$$

Comparison of Eqs. (2.9) and (2.11) shows that we may express the elements of the deuteron-scattering matrix, Eq. (2.8), in terms of the elements of the nucleon-scattering matrix Eq. (2.10) at the same momentum transfer:

$$g_d(K)=\left(\frac{\mu_d}{\mu_n}\right)g_n(K),$$
$$h_d(K,k_d)=\left(\frac{k_d}{k_n}\right)^2\left(\frac{\sin\theta_d}{\sin\theta_n}\right)\left(\frac{\mu_d}{\mu_n}\right)h_n(K,k_n). \quad (2.12)$$

[6] Note that the sign of the $\langle T_{21}\rangle$ term is incorrect in Lakin's paper.
[7] G. F. Chew, Phys. Rev. **80**, 196 (1950); G. F. Chew and G. C. Wick, Phys. Rev. **85**, 636 (1952).
[8] G. F. Chew, Phys. Rev. **74**, 809 (1948).
[9] K. A. Brueckner, Phys. Rev. **89**, 834 (1953).
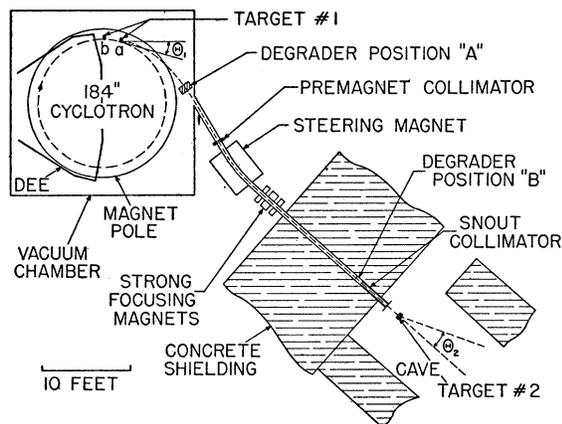
FIG. 1. Celebrated figure showing plan view of cyclotron and path of polarized beam.

Later we will compare the predictions of the above approximation with our experimental results. We will estimate $g_n(K)$ and $h_n(K,k_n)$, using the results of proton-nucleus scattering experiments. In the scattering of deuterons of momentum k_d, the nucleons that compose the deuteron interact with the target nucleus at an average momentum $k_n=k_d/2$. (This is smeared out because of the internal momentum of the deuteron.) In making our comparison, then, we must use proton experiments at an energy about half that of the associated deuteron results.

Lakin shows that Eq. (2.8) yields

$$I_0 = f[4|g_d|^2 + \tfrac{2}{3}|h_d|^2],$$

$$I_0 i\langle T_{11}\rangle = \frac{2}{\sqrt{3}}f(g_d^* h_d + g_d h_d^*), \qquad (2.13)$$

$$I_0\langle T_{21}\rangle = 0.$$

Equations (2.12) and (2.13) enable us to express the parameters characterizing deuteron-nucleus double scattering in terms of the proton-nucleus scattering matrix at the same center-of-mass momentum transfer, K. We refer to them again in the discussion of the results.

3. EXPERIMENTAL

The experimental arrangement was similar to that used for the double scattering of protons, described in a previous paper.[10]

A. Polarized Beam

The 165-Mev polarized deuteron beam was obtained by scattering the 190-Mev internal circulating deuteron beam from a target (target No. 1) inside the 184-inch cyclotron vacuum tank. The particles scattered outward were deflected in the fringing field of the cyclotron.

Those particles which were scattered at a suitable angle passed through an aperture in the vacuum tank into an evacuated exit tube. The beam entered the experimental area (cave) through a tubular collimator (snout collimator) 46 inches long. The first scattering was done from position a of Fig. 1. Calculations indicated that deuterons scattered at an angle of 17° would reach the exit tube. After the cyclotron had been shut down for conversion, however, measurements made with a mechanical analog orbit plotter determined the first-scattering angle to be 16°±0.5°. The error in the first scattering angle corresponding to a $\tfrac{1}{2}$-inch radial error in target position was determined to be about 1° and this value represents an estimate of the maximum error in the first-scattering angle.

B. Energy Degradation

To obtain the 133- and 100-Mev beams, it was necessary to degrade the full-energy polarized beam. The degradation was done inside the vacuum tank by placing beryllium bricks at position A of Fig. 1. Beryllium was used to minimize intensity loss due to multiple scattering. The change of beam polarization due to the degradation process has been calculated by Wolfenstein[11] and shown to be negligible. We have also considered the possibility that, owing to the changed magnetic rigidity of the particles after they have passed through the degrader, the exit tube might accept particles whose first-scattering angle is different from the assumed one. Calculations indicate that this effect is also small. An experimental check using the polarized proton beam has been performed[12] and seems to confirm the expectation that the polarization of the degraded beam is substantially the same as that of the full-energy beam.

C. Apparatus

To measure the scattered intensity, a three-counter telescope was used. These counters were called Counters 1, 2 and 3, number 1 being defining and closest to the target. A variable copper absorber was put between Counters 1 and 2. A small fixed absorber was sometimes inserted between Counters 2 and 3. The coincidence circuit used was capable of detecting simultaneously, 1-2-3 and 1-2 coincidences. In all the runs, a snout collimator of circular cross section was used in order to obtain a beam with high azimuthal symmetry. A 1-inch-diameter collimator was used when possible, in order to obtain good angular and energy resolution. However, on the low-energy experiments we used a 2-inch-diameter collimator in order to obtain sufficient beam intensity.

D. Counting Procedure

For each polar angle Θ and azimuthal angle ϕ, three counting rates were measured. These consisted of

[10] Chamberlain, Segrè, Tripp, Wiegand, and Ypsilantis, Phys. Rev. 102, 1659 (1956).

[11] L. Wolfenstein, Phys. Rev. 75, 1664 (1949).
[12] D. Fischer and J. Baldwin, Phys. Rev. 100, 1445 (1955).

"target in," "target out," and accidental coincidence counting rates. The accidental rate was measured with the target in place and with a time delay equal to the cyclotron rf pulse repetition time introduced into the circuit of counter No. 1. This rate was generally negligible. The counting rate due to the target, $\mathcal{J}(\Theta,\phi)$,[13] was obtained through the relation

$$\mathcal{J}(\Theta,\phi) = (\text{target in}) - (\text{target out}) - (\text{accidental}). \quad (3.1)$$

The counting rates were used to derive three quantities. These are:

(a) the coefficient of $\cos\phi$ in the angular distribution, denoted by e:

$$e(\Theta) = \frac{\mathcal{J}(\Theta,0°) - \mathcal{J}(\Theta,180°)}{\mathcal{J}(\Theta,0°) + \mathcal{J}(\Theta,180°)}; \quad (3.2)$$

(b) the coefficient of $\cos2\phi$, denoted by B:

$$B(\Theta)$$
$$= \frac{[\mathcal{J}(\Theta,0°) + \mathcal{J}(\Theta,180°)] - [\mathcal{J}(\Theta,90°) + \mathcal{J}(\Theta,270°)]}{[\mathcal{J}(\Theta,0°) + \mathcal{J}(\Theta,180°)] + [\mathcal{J}(\Theta,90°) + \mathcal{J}(\Theta,270°)]};$$
$$(3.3)$$

(c) the average counting rate, denoted by $\mathcal{J}_{Av}$:

$$\mathcal{J}_{Av}(\Theta) = \tfrac{1}{4}[\mathcal{J}(\Theta,0°) + \mathcal{J}(\Theta,90°) + \mathcal{J}(\Theta,180°) + \mathcal{J}(\Theta,270°)]. \quad (3.4)$$

Since the first scattering is to the left, $\phi=0°$ is defined as scattering to the left, $\phi=90°$ is scattering up, etc.

The angular distribution observed with an unpolarized beam is called $\mathcal{J}_0(\Theta)$. The second scattered angular distribution is expressed in terms of the experimental parameters α, B, e, and $\mathcal{J}_0$ as

$$\mathcal{J} = \mathcal{J}_0[1 + \alpha + e\cos\phi + B\cos2\phi], \quad (3.5)$$

and in terms of theoretical parameters by Eq. (2.2). Explicitly, the correspondence between the theoretical and experimental parameters is

$$\alpha = \langle T_{20}\rangle_1 \langle T_{20}\rangle_2,$$
$$e = 2[-\langle T_{21}\rangle_1 \langle T_{21}\rangle_2 + i\langle T_{11}\rangle_1 i\langle T_{11}\rangle_2], \quad (3.6)$$
$$B = 2\langle T_{22}\rangle_1 \langle T_{22}\rangle_2.$$

The measurement of α required two separate experiments, one with a polarized beam and one with an unpolarized beam. For a polarized beam we have

$$(\mathcal{J}_{Av})_p = \tfrac{1}{4}[\mathcal{J}(0°) + \mathcal{J}(90°) + \mathcal{J}(180°) + \mathcal{J}(270°)] = \mathcal{J}_0(1 + \alpha), \quad (3.7)$$

and for an unpolarized beam,

$$(\mathcal{J}_{Av})_u = \mathcal{J}_0. \quad (3.8)$$

Thus

$$\alpha = [(\mathcal{J}_{Av})_p / (\mathcal{J}_{Av})_u] - 1. \quad (3.9)$$

In order to make the two experiments as similar as possible, special precautions were taken. The same target and telescope absorber were used in both measurements. The unpolarized beam had a higher energy and smaller energy spread than the polarized beam. To rectify this, a carbon wedge was placed in the beam at position A of Fig. 1. Bragg-curve measurements[14] determined the polarized beam energy as 165 ± 3.1 Mev and the degraded unpolarized beam energy as 165 ± 2.8 Mev. A copper, rather than a carbon, first target was used in the hope that the smaller diffraction pattern would result in larger $\langle T_{20}\rangle$ at the first scattering angle.

E. Angular Resolution

The geometrical angular resolution was computed by folding together the effects of a circular aperture due to the beam size and a rectangular aperture due to the defining counter. The effect of multiple Coulomb scattering was taken from Millburn and Schecter.[15] The total angular resolution was obtained by taking the square root of the sum of the squares of the two rms angles. The results agreed reasonably well with the values obtained experimentally by sweeping the counters through the beam.

F. Beam Polarization

In the appendix we discuss the effect that the magnetic fields encountered by the polarized beam have on the beam polarization. There is no effect on the vector polarization, $i\langle T_{11}\rangle$. The fields do, however, produce a mixing $\langle T_{2M}\rangle$. From Eq. (A.1), we see that for the conditions of this experiment the effect is small and can be neglected.

The only nonzero $\langle T_{JM}\rangle$ that we have uncovered are related to the asymmetry by the second of Eqs. (3.6). If one performed an experiment in which the polarized beam was deflected through a large angle by means of a magnetic field, he could determine how much of e was produced by $\langle T_{21}\rangle$ and how much by $i\langle T_{11}\rangle$. Such an experiment was not done because of the extremely large deflections required (see appendix). It is therefore impossible to disentangle, in the measured asymmetry, the parameters characterizing the first and second scatterings. We would like to go further than simply listing the observed asymmetries and to this end we shall make the heuristic assumption that $|\langle T_{21}\rangle| \ll 1$ at the angle of the first scattering. This allows us to say $\langle T_{21}\rangle_1 \langle T_{21}\rangle_2 \approx 0$. The following considerations support this assumption. The first Born approximation predicts $\langle T_{21}\rangle \equiv 0$. The more extensive calculations by Stapp[5] indicate that

---

[13] In general, we use the symbol $\mathcal{J}$ to denote a scattered intensity, and the symbol I for a differential scattering cross section. In cases where the distinction is unimportant, we use the symbol I interchangeably.

[14] Chamberlain, Segrè, and Wiegand, Phys. Rev. 83, 923 (1951).
[15] G. P. Millburn and L. Schecter, University of California Radiation Laboratory Report UCRL-2234, January, 1954 (unpublished).

TABLE I. Estimate of rms systematic error in asymmetry. E is the beam energy.

E (Mev)	Target No. 2	Θ	$(\delta e)_{rms}$	E (Mev)	Target No. 2	Θ	$(\delta e)_{rms}$
165	C	9	0.084	100	C	4	0.104
		10	0.069			7	0.061
		11	0.065			10	0.030
		14	0.041			14	0.067
		17	0.029			18	0.010
		18	0.029			22	0.009
		20	0.025			26	0.025
		24	0.025			30	0.022
		28	0.025			34	0.019
	Al	8	0.072		Al	4	0.207
		12	0.032			7	0.076
		16	0.021			10	0.062
		18	0.035			14	0.023
		20	0.042			18	0.000
		24	0.023			22	0.031
		28	0.023			26	0.014
		32	0.023			30	0.015
						34	0.021
	Cu	17	0.026				
		21	0.034				
		25	0.027				
133	C	4	0.056				
		7	0.049				
		10	0.049				
		14	0.040				
		18	0.011				
		22	0.025				
		26	0.025				
		30	0.025				
	Be	14	0.021				
		18	0.027				
		22	0.030				
		26	0.016				

$\langle T_{21}\rangle$ should be small compared with $i\langle T_{11}\rangle$. The experiment reported here shows that the other $\langle T_{2M}\rangle$ are small. Consistent with this assumption, the asymmetry may now be written as

$$e = 2i\langle T_{11}\rangle_1 i\langle T_{11}\rangle_2 = \tfrac{3}{2}\langle S_y\rangle_1\langle S_y\rangle_2. \qquad (3.10)$$

We now have a relation that looks very similar to that applying to particles of spin $\tfrac{1}{2}$, in which e depends on the product of a number characteristic of the beam multiplied by another characteristic of the target. We may now speak of a beam polarization (referring to the value of $i\langle T_{11}\rangle$ characterizing the beam) and list values of $i\langle T_{11}\rangle$ for various targets, energies, and scattering angles. No information has been obtained concerning the absolute sign of the polarization.

The errors given for the tabulated values of $i\langle T_{11}\rangle$ include the estimated systematic error in the determination of the polarization of the incident deuteron beam as well as the statistical error in the measurement of the asymmetry (see Table V). All errors reported are standard deviations.

One other point should be mentioned. The polarized proton beam was usually obtained by scattering at $\sim 10°$ from Be. The polarization changes about 4.5% per degree in this region. In the deuteron experiments,

we most commonly used C at $16°$ where $i\langle T_{11}\rangle$ is changing about 15.5% per degree. This makes the deuteron results more strongly dependent upon errors in first-target position, cyclotron main field, etc.

G. Discussion of Uncertainties

The absolute values of I_0 are uncertain to about 20%. This is chiefly due to the uncertainties contained in the extrapolation of the counting rate to zero absorber and the slope of the voltage plateaus. Because of the preponderance of inelastic scattering at large angles, the tabulated values of I_0 must there be interpreted as, at best, upper limits to the true values of the elastic cross sections. The errors quoted are derived from counting statistics alone.

The asymmetries found with the unpolarized beam in the α experiment can be used to make an estimate of the systematic error in e in the following way. Let us assume that the asymmetries calculated from the unpolarized data are due to small misalignment errors. If we define

$$\beta(\Theta) = \frac{d}{d\Theta}\ln I_0(\Theta),$$

then, to first order and for $e^2 \ll 1$, the error δe produced in the asymmetry by an angular misalignment $\delta\Theta$ is given by $\delta e = \beta\delta\Theta$. From the asymmetries observed with the unpolarized beam, we compute $(\delta\Theta)_{rms} \simeq 0.14°$. Using this value of $(\delta\Theta)_{rms}$, we obtain values of $(\delta e)_{rms} = \beta(\delta\Theta)_{rms}$ for our data. These are listed in Table I.

One may also compute values of B for the unpolarized beam. These are listed in Table II. Four of the eight measured are greater than their statistical uncertainties, the worst being about 1.7 times its uncertainty. Thus we are inclined to believe that in the experiments with the polarized beam (see Table III) we have observed no values of B inconsistent with zero.

The α experiment depends critically on matching the beam energies and energy spreads of the polarized and unpolarized deuteron beams. Although the counting rate due to elastic scattering should be independent of small variations of beam energy, that due to inelastic scattering is not. Crude estimates of the inelastic contamination at $\Theta = 17°$ indicate that a disparity in

TABLE II. Values of B observed with unpolarized beam.

Target	Θ	$|B|$
C	9	0.0013 ± 0.0085
	11	0.0049 ± 0.0088
	17	0.0088 ± 0.0095
	17	0.0135 ± 0.0087
Cu	17	0.0114 ± 0.0078
	17	0.0086 ± 0.0082
	21	0.0065 ± 0.0110
	25	0.0197 ± 0.0117

TABLE III. Cross sections, asymmetries, polarizations, etc., for deuterons elastically scattered from lithium, beryllium, carbon, aluminum, and copper.

Θ[a] (degrees)	I_0[b] (mb/sterad)	e[c]	B[d]	$i\langle T_{11}\rangle$[e]	Target 1	Group[f]
			Carbon $\sim$156 Mev			
9	1557 ± 13	-0.010 ± 0.012	$+0.016\pm0.008$	-0.017 ± 0.020	Cu	III
10	877 ± 7	$+0.017\pm0.011$	-0.004 ± 0.012	$+0.027\pm0.017$	Al	I
11	575 ± 3	0.041 ± 0.008	$+0.007\pm0.006$	0.062 ± 0.013	C	I
11	575 ± 8	0.078 ± 0.014	-0.008 ± 0.090	0.117 ± 0.022	C	II
14	163 ± 3	0.155 ± 0.021	$+0.042\pm0.016$	0.242 ± 0.034	Al	I
17	94.2 ± 2.1	0.319 ± 0.022	$+0.001\pm0.020$	0.480 ± 0.046	C	II
17	103.6 ± 1.0	0.253 ± 0.011		0.480 ± 0.055	C	IV
18	82.0 ± 1.3	0.283 ± 0.028		0.426 ± 0.052	C	I
18		0.287 ± 0.019	$+0.019\pm0.035$	0.448 ± 0.035	Al	I
20	54.7 ± 0.5	0.332 ± 0.019	-0.004 ± 0.014	0.499 ± 0.044	C	I
24	25.9 ± 0.7	0.317 ± 0.035		0.495 ± 0.058	Al	I
28	12.5 ± 0.4	0.279 ± 0.028		0.528 ± 0.078	C	IV
			Aluminum $\sim$157 Mev			
8	2545 ± 24	-0.033 ± 0.021		-0.049 ± 0.031	C	I
12	400 ± 5	$+0.225\pm0.012$	-0.019 ± 0.012	$+0.339\pm0.029$	C	I
16	242 ± 1	0.233 ± 0.012	-0.004 ± 0.011	0.351 ± 0.030	C	I
16		0.205 ± 0.016		0.320 ± 0.013	Al	I
18	160 ± 2	0.226 ± 0.009		0.353 ± 0.020	Al	I
20	84.6 ± 1.4	0.281 ± 0.030	$+0.008\pm0.008$	0.422 ± 0.053	C	I
20		0.278 ± 0.031		0.434 ± 0.051	Al	I
24	36.6 ± 0.8	0.450 ± 0.048		0.677 ± 0.085	C	I
28	19.5 ± 1.0	0.454 ± 0.069		0.682 ± 0.134	C	I
32	9.30 ± 0.37	0.378 ± 0.049		0.567 ± 0.083	C	I
			Copper $\sim$157 Mev			
17	201 ± 8	0.238 ± 0.038	$+0.016\pm0.027$	0.357 ± 0.062	C	II
17	222 ± 2	0.231 ± 0.041	$+0.002\pm0.025$	0.389 ± 0.097	Cu	III
21	111 ± 6	0.299 ± 0.053	$+0.052\pm0.037$	0.450 ± 0.086	C	II
21	105 ± 4	0.335 ± 0.040	$+0.006\pm0.026$	0.503 ± 0.069	C	II
21	121 ± 1	0.272 ± 0.053	$+0.061\pm0.038$	0.457 ± 0.119	Cu	III
25	40.1 ± 2.3	0.384 ± 0.059	$+0.011\pm0.042$	0.577 ± 0.097	C	II
			Lithium $\sim$121 Mev			
22	44.5 ± 1.1	0.217 ± 0.025		0.410 ± 0.064	C	VI
			Beryllium $\sim$124 Mev			
14	302 ± 5	0.045 ± 0.017		0.084 ± 0.033	C	VI
18	105 ± 2	0.164 ± 0.021		0.310 ± 0.052	C	VI
22	55.5 ± 1.3	0.273 ± 0.024		0.517 ± 0.071	C	VI
26	29.7 ± 1.1	0.255 ± 0.037		0.483 ± 0.087	C	VI
			Carbon $\sim$125 Mev			
4	$12\,500\pm200$	-0.016 ± 0.018		-0.031 ± 0.035	C	VI
7	3860 ± 20	$+0.033\pm0.019$		$+0.063\pm0.037$	C	VI
10	1400 ± 20	0.023 ± 0.014		0.044 ± 0.027	C	VI
14	275 ± 7	0.108 ± 0.024		0.205 ± 0.050	C	VI
18	$130+4$	0.280 ± 0.032		0.530 ± 0.083	C	VI
18	130 ± 3	0.222 ± 0.020		0.420 ± 0.059	C	VI'
22	77.0 ± 1.9	0.256 ± 0.027		0.484 ± 0.073	C	VI
26	37.6 ± 1.1	0.323 ± 0.031		0.612 ± 0.087	C	VI'
30	17.9 ± 0.8	0.333 ± 0.042		0.631 ± 0.104	C	VI'
			Carbon $\sim$94 Mev			
4	$27\,900\pm600$	-0.037 ± 0.019		-0.070 ± 0.037	C	V
7	4350 ± 40	-0.055 ± 0.009		-0.104 ± 0.020	C	V
10	1770 ± 20	-0.071 ± 0.009		-0.135 ± 0.023	C	V
14	452 ± 8	-0.032 ± 0.019		-0.060 ± 0.036	C	V
14	438 ± 8	-0.069 ± 0.019		-0.130 ± 0.038	C	V
18	169 ± 4	$+0.095\pm0.023$		$+0.180\pm0.048$	C	V
22	152 ± 3	$+0.099\pm0.022$		$+0.188\pm0.046$	C	V
26	91.5 ± 2.5	0.131 ± 0.028		0.249 ± 0.059	C	V
30	47.0 ± 1.3	0.164 ± 0.028		0.311 ± 0.062	C	V
34	24.4 ± 1.3	0.253 ± 0.051		0.480 ± 0.110	C	V
			Aluminum $\sim$94 Mev			
4	$118\,000\pm1000$	$+0.020\pm0.010$		$+0.038\pm0.019$	C	V
7	6650 ± 70	-0.082 ± 0.011		-0.155 ± 0.026	C	V
10	1510 ± 20	-0.097 ± 0.016		-0.184 ± 0.036	C	V
14	388 ± 9	$+0.012\pm0.023$		$+0.022\pm0.044$	C	V
18	366 ± 9	-0.039 ± 0.024		-0.074 ± 0.045	C	V
22	212 ± 5	-0.020 ± 0.020		-0.038 ± 0.042	C	V
26	97.4 ± 2.9	$+0.105\pm0.029$		$+0.199\pm0.059$	C	V
30	73.1 ± 3.3	$+0.212\pm0.046$		$+0.401\pm0.096$	C	V
34	42.7 ± 2.5	$+0.170\pm0.060$		$+0.322\pm0.118$	C	V

a Θ: second-scattering angle in laboratory system.
b I_0: unpolarized differential scattering cross section (lab). Errors quoted are due to counting statistics only. The absolute cross section is good to about 20%.
c e: asymmetry. Quoted errors are due to counting statistics only.
d B: errors due to counting statistics only. See Sec. 3-D.
e $i\langle T_{11}\rangle$: vector-type polarization. Errors include beam polarization statistics.
f Group: group designation (correlates data with those of Table VI).
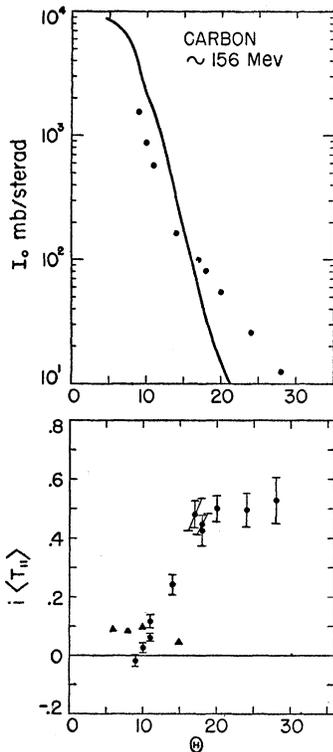
FIG. 2. Scattering of 156-Mev deuterons from carbon. Upper curve: cross section; lower curve: vector polarization. Triangular points and solid curve are predictions from proton data.

beam energies of 1 Mev can give rise to an error of 0.002 in α. It is reasonable to suppose that drift in the steering-magnet field and main cyclotron field could
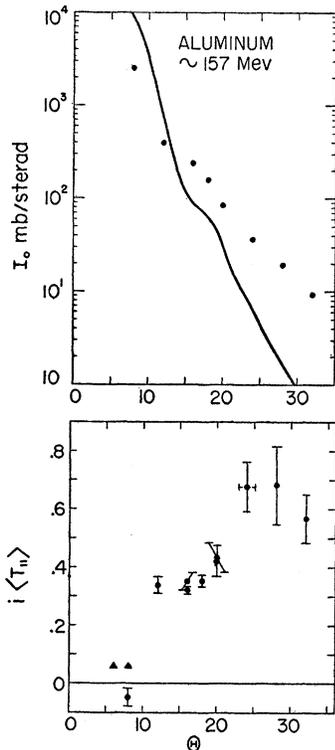
FIG. 3. Scattering of 157-Mev deuterons from aluminum. Upper curve: cross section; lower curve: vector polarization. Triangular points and solid curve are predictions from proton data.

give rise to a change in beam energy of at least 0.5 Mev. Thus, the experimental results (see Table IV) are consistent with $\alpha=0$.

4. DISCUSSION OF RESULTS

The results appear in Table III and IV and in Figs. 2 through 8. Beam polarizations are given in Table V. The data are divided into groups. Each time a critical parameter (snout collimator diameter, beam energy, etc.) was changed, a new group designation was assigned. Table VI gives the parameters characterizing each group as well as target thickness, rms angular resolution, and mean scattering energy for each of the experiments within the group.

Let us now compare our results with the predictions of the impulse approximation. We make use of the Harvard unpolarized differential cross-section measurements for the scattering of protons from carbon and

TABLE IV. Values of α. (See Sec. 3-D.) $\bar{E}$ is the mean scattering energy. The first scattering was from a copper target. Errors quoted are due to counting statistics only. The unpolarized beam is Group III' and the polarized beam Group III.

Target 2	Θ	α	$\bar{E}$ (Mev)
C	9°	$+0.005\pm0.010$	159
Cu	17°	$+0.026\pm0.027$	157
Cu	21°	-0.016 ± 0.038	157

TABLE V. Beam polarizations. D is the diameter of the snout collimator. Errors are due to counting statistics only.

Target 1	D (in.)	$i\langle T_{11}\rangle_1$	
C	1	0.333 ± 0.022	
Al	1	0.320 ± 0.013	Groups I–III
Cu	1	0.298 ± 0.052	
C	2	0.264 ± 0.028	Groups IV–VI'

aluminum near 90 Mev,[16] and the Harwell low-energy polarization data for carbon and aluminum.[17]

The following expressions relate g_n and h_n of the nucleon-nucleus scattering matrix (2.10) to the quantities measurable at this energy:

$$I_0{}^n = |g_n|^2 + |h_n|^2,$$
$$I_0{}^n P = g_n{}^* h_n + g_n h_n{}^*. \qquad (4.1)$$

Here $I_0{}^n$ is the nucleon-nucleus unpolarized scattering cross section and P is the polarization.[18] It will be seen by referring to Eqs. (2.12) and (2.13) that g and h enter the expressions for $I_0{}^d$ and $I_0{}^n$ in different ways. We

---

[16] K. Strauch and F. Titus, Phys. Rev. 103, 200 (1956); Gerstein, Niederer, and Strauch (private communication).
[17] Dickson, Rose, and Salter, Proc. Phys. Soc. (London) A68, 361 (1955) and private communication.
[18] It might be well at this point to underline the similarity between $i\langle T_{11}\rangle$ and P. Both are expectation values of spin operators. They point along the normal to the first-scattering plane. The same mechanism gives rise to each of them and both are proportional to $I_0^{-1}(g^*h+gh^*)$.

cannot predict $I_0{}^d$ from $I_0{}^n$ without a simplifying assumption. In view of the smallness of P at these energies, it is reasonable to assume that $|h|^2 \ll |g|^2$. On this basis we have

$$I_0{}^d(K) = 4f(K)\left(\frac{\mu_d}{\mu_n}\right)^2 I_0{}^n(K). \qquad (4.2)$$

This appears as the solid curve in Figs. 2 and 3 (upper). Using these expression for $I_0{}^d$, we obtain $i\langle T_{11}\rangle$ in terms of the nucleon polarization P for the same momentum transfer K as

$$i\langle T_{11}\rangle = \frac{2}{\sqrt{3}} \times \frac{1}{4}\left(\frac{k_d}{k_n}\right)^2\left(\frac{\sin\theta_d}{\sin\theta_n}\right)P(K). \qquad (4.3)$$

The results of this calculation appear as the triangular points in Figs. 2 and 3 (lower).

The agreement is quantitatively poor. The theory predicts that $i\langle T_{11}\rangle \simeq 3^{-\frac{1}{2}}$ times the polarization for

TABLE VI. Parameters of the scattering. E is beam energy in Mev; Intens. is beam intensity in deuterons per second; D is diam. of snout collimator; t is thickness of second target; $\bar{E}$ is mean scattering energy; $\Delta\Theta$ is rms angular resolution.

Group	E (Mev)	Intens. (d/sec)	D (in.)	Target 1	Target 2	t (g/cm²)	$\bar{E}$ (Mev)	$\Delta\Theta$ (degrees)
I	165±2.6	8×10⁴	1	C and Al	C	2.25	156	0.91
					Al	2.57	156	1.13
II	165±3.4	8×10⁴	1	C	C	1.59	159	0.83
					Cu	2.83	157	1.46
III	165±3.1	4×10⁴	1	Cu	C	1.59	159	0.83
					Cu	2.83	157	1.46
III'	165±2.8	⋯	1	⋯	C	1.59	159	0.83
					Cu	2.83	157	1.46
IV	160±5.5	5×10⁵	2	C	C	2.25	151	1.20
V	100±5.9	8×10⁴	2	C	C	1.00	94	1.21
					Al	1.29	94	1.45
VI	133±4.5	5×10⁴	2	C	Li	2.83	121	1.22
					Be	2.12	124	1.18
					C	1.00	128	1.11
VI'	133±4.5	5×10⁴	2	C	C	2.00	124	1.26

nucleons at half the deuteron energy. Proton polarizations are notoriously small below 95 Mev, whereas $i\langle T_{11}\rangle$ becomes respectably large at large scattering angles. The values of $i\langle T_{11}\rangle$ at 24° and 28° for aluminum at 157 Mev are near $2^{-\frac{1}{2}}$, which is the maximum value attainable if $\langle T_{21}\rangle = 0$.

Nor is there qualitative agreement. Since P should vary as $\sin\theta$ for small θ, the theory does not predict the observed change of sign of $i\langle T_{11}\rangle$ at small angles.[19,20] The observed and predicted values of $I_0{}^d$ for carbon seem to run parallel to each other at small angles. At larger angles the observed values fall off much less rapidly than the predicted. The same sort of behavior is observed with aluminum.

It is interesting to plot $i\langle T_{11}\rangle$ is such a way as to facilitate the comparison of our results at different

[19] It is not likely that this rapid fall of $i\langle T_{11}\rangle$ as θ decreases is due to Coulomb scattering. The cross-section data from Harvard indicate that Coulomb scattering becomes important at angles much smaller than any at which we have made measurements.
[20] W. Heckrotte, Phys. Rev. **101**, 1406 (1955).
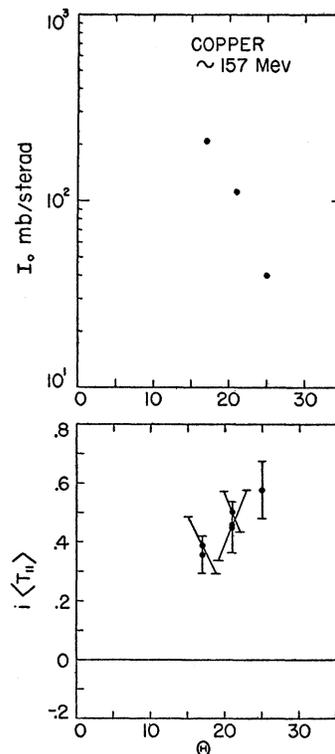
FIG. 4. Scattering of 157-Mev deuterons from copper. Upper curve: cross section; lower curve: vector polarization.

energies and for different target nuclei. In Fig. 9 we have passed a smooth curve through the experimental values, using as abscissa the value of the momentum
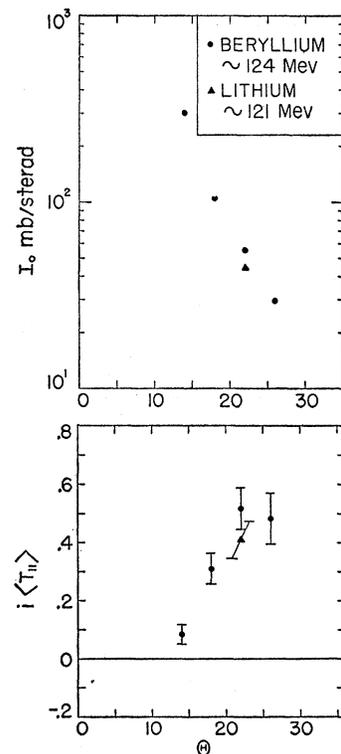
FIG. 5. Scattering of 124-Mev deuterons from beryllium and 121-Mev deuterons from lithium. Upper curve: cross section; lower curve: vector polarization.
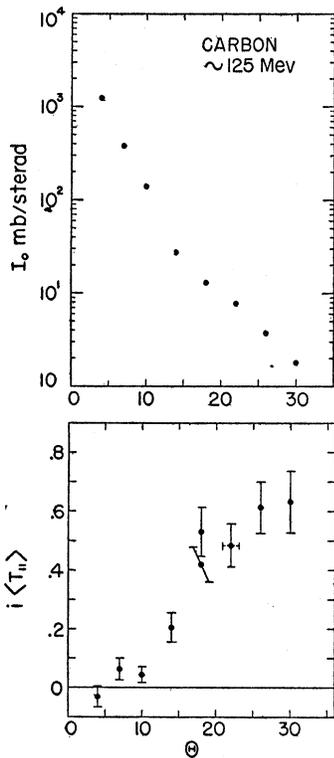
FIG. 6. Scattering of 125-Mev deuterons from carbon. Upper curve: cross section; lower curve: vector polarization.

transfer times the cube root of the target mass number. It is seen that there is a good deal of similarity between the curves. The rapid fall-off of $i\langle T_{11}\rangle$ is a quite con-
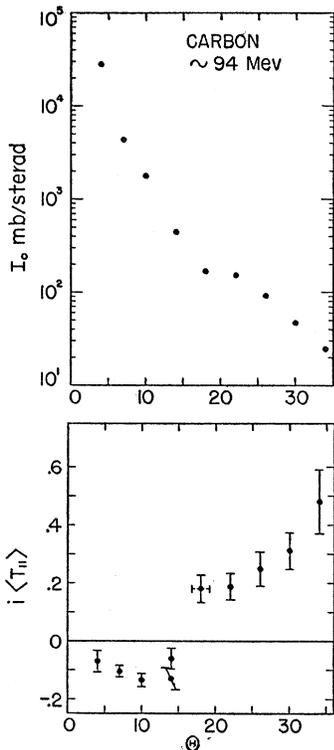
FIG. 7. Scattering of 94-Mev deuterons from carbon. Upper curve: cross section; lower curve: vector polarization.

sistent feature, and is centered in all cases around $KA^{\frac{1}{3}}=2$. The lowering of the energy from 156 to 94 Mev seems to result in a general depression of $i\langle T_{11}\rangle$.

The reason for the disparity between the theoretical and experimental results is not known. It is unlikely that the trouble can be traced to multiple collisions of a single nucleon within the target nucleus, since we have used empirically derived nucleon amplitudes in our calculations. Professor Malvin A. Ruderman has attempted to use the presence of D state in the deuteron wave function to explain the change of sign of the polarization at small angles, with very little success so far. It is possible that inclusion in the theory of the possibility for simultaneous scatter-
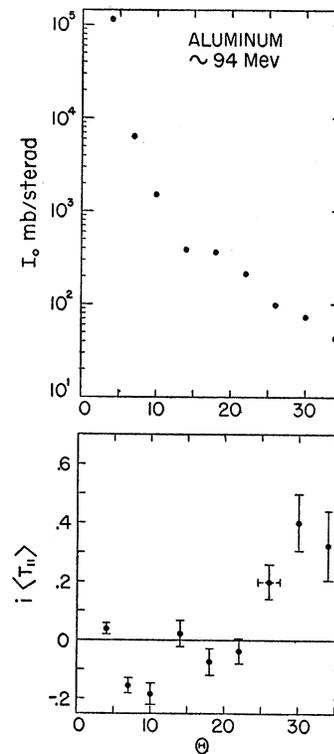
FIG. 8. Scattering of 94-Mev deuterons from aluminum. Upper curve: cross section; lower curve: vector polarization.

ing of both nucleons of the deuteron would lead to enhancement of the large-angle cross section and polarization. There is one other refinement of the impulse approximation, which is suggested by the following observations. An imaginary part is usually included in the nucleon-nucleus potential. This is used to describe the effect of inelastic events in which the target nucleus is left in an excited state. We would expect to find, in the equivalent deuteron-nucleus potential, an additional imaginary part describing inelastic events in which the deuteron was dissociated. The impulse approximation does not seem to predict this feature. The inclusion of the attenuation of the deuteron wave by this sort of stripping reaction as the wave traverses the target nucleus should also lead to
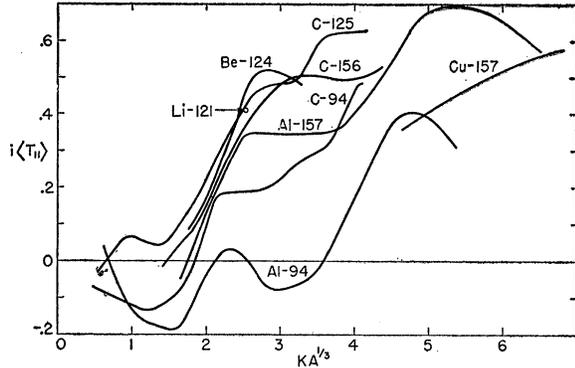
FIG. 9. Composite of all $i\langle T_{11}\rangle$ data, plotted against $KA^{\frac{1}{3}}$ $=2kA^{\frac{1}{3}}\sin\frac{1}{2}\theta$. The number following the element symbol is the mean scattering energy in Mev.

enhancement of the large-angle polarization. Although the consideration of these two effects should operate to reduce the difference between theory and experiment, we ·do not know whether it results in quantitative agreement. Indeed, it is very unlikely that we can, by this means, explain the small-angle change of the sign of the polarization.

5. ACKNOWLEDGMENTS

APPENDIX. EFFECT OF A MAGNETIC FIELD ON THE DEUTERON SPIN STATE

The fringing field of the cyclotron and the field of the bending magnet, as they are parallel to the normal of the first scattering plane, do not affect the value of $i\langle T_{11}\rangle$ characterizing the beam. These fields do, however, produce a mixing of the $\langle T_{2M}\rangle$. Two factors contribute to this effect. (1) The $\langle T_{2M}\rangle_1$ which result which result from the first scattering are referred to a set of coordinates having z axis along $\mathbf{k}_{1f}$, whereas we must refer them to coordinates having z axis along $\mathbf{k}_{2i}$—the direction in which the beam actually enters the cave. (2) The effect of the magnetic field on the spins themselves is to rotate the principal axes of the tensor $\langle S_i S_j\rangle$. These two effects produce the same result on the $\langle T_{2M}\rangle$, but in opposite directions and with different magnitudes.

If we designate that $\langle T_{2M}\rangle$ resulting from the first scattering and referred to a z axis along $\mathbf{k}_{1f}$, simply as $\langle T_{2M}\rangle$, and the $\langle T_{2M}\rangle$ of the beam entering the cave and referred to a z axis along $\mathbf{k}_{2i}$ as $\langle T_{2M}\rangle'$, then

$$\langle T_{22}\rangle' = \tfrac{1}{2}(1+\cos^2\lambda)\langle T_{22}\rangle - \tfrac{1}{2}\sin2\lambda\langle T_{21}\rangle$$
$$+\tfrac{1}{2}(\tfrac{3}{2})^{\frac{1}{2}}\sin^2\lambda\langle T_{20}\rangle,$$

$$\langle T_{21}\rangle' = \tfrac{1}{2}\sin2\lambda\langle T_{22}\rangle + \cos2\lambda\langle T_{21}\rangle$$
$$-\tfrac{1}{2}(\tfrac{3}{2})^{\frac{1}{2}}\sin2\lambda\langle T_{20}\rangle, \quad (A.1)$$

$$\langle T_{20}\rangle' = (\tfrac{3}{2})^{\frac{1}{2}}\sin^2\lambda\langle T_{22}\rangle + (\tfrac{3}{2})^{\frac{1}{2}}\sin2\lambda\langle T_{21}\rangle$$
$$+(1-\tfrac{3}{2}\sin^2\lambda)\langle T_{20}\rangle,$$

where $\lambda = (\mu-1)\eta$, $\mu = +0.85647 =$ deuteron magnetic moment, in nuclear magnetons, and $\eta =$ the total angular deflection of the beam, considered positive when directed opposite to the normal, $\mathbf{n}_1$, to the first-scattering plane. In this experiment, $\eta = 39.5°$ and $\lambda = -5.67°$.